

RESEARCH PAPER

The Influence of Rotor Converters on the Behavior of Static Rotor Resistance Control of Induction Motor under Supply Voltages Asymmetry

Hilmi Fadhil Ameen¹

1Department of Electrical Engineering, College of Engineering, Salahaddin University-Erbil, Kurdistan Region, Iraq

ABSTRACT

This paper examines the impact of harmonics generated by the power semiconductor devices in the rotor circuit of a Softly Rotor Resistance Variation Induction Motor Drive System (SRRVIMDS) operating under voltage asymmetry. The study evaluates the components of rotor currents, electromagnetic torque, and stator winding currents based on a detailed mathematical circuit model configuration. The analysis also investigates the stator winding distortion currents produced by electromagnetic induction in the stator windings due to the harmonic components of the rotor current. The paper provides relationships for estimating all harmonic order frequencies of the stator currents, rotor currents, and torque as a function of the stator frequency and rotor speed. The results show that the investigated currents have sufficient accuracy, except at a slip of one-sixth, where notable differences occur.

KEY WORDS: Softly Rotor Resistance Variation Induction Motor (SRRVIM), Chopper Circuit, Voltage Asymmetry, Frequency Spectrum Analysis.

DOI: <http://dx.doi.org/10.21271/ZJPAS.35.5.3>

ZJPAS (2023) , 35(5);24-39 .

1. INTRODUCTION

The behavior of the SRRVIMDS is influenced by rotor power semiconductor converters due to their effect on the supply voltage asymmetry. The SRRVIMDS is a method for controlling the speed of a wound rotor induction motor by adjusting the resistance in the rotor circuit to verify the required performance. Typical applications for the speed control of a slip ring induction motor are conveyer belts, mills, crushers, mixers, agitators, etc. The use of slip power dissipation in a constant outer resistance via a DC chopper provides a very interesting solution when slip power dissipation does not exceed several hundred kW and for drives requiring accurate and fast speed response. The rotor resistance is adjusted by means of a chopper circuit, which is a switch that controls the flow of current in the rotor circuit.

This method is relatively simple and cost-effective, and it can be used to achieve smooth and precise speed control. However, it may result in increased losses in the rotor circuit, reducing the motor's efficiency. The presence of a three-phase bridge rectifier and chopper circuit in the rotor circuit of a wound-rotor induction motor can negatively impact its performance. The harmonics can cause increased losses and heating in the motor, leading to reduced efficiency and a shorter lifespan. Additionally, they can generate electromagnetic interference, causing errors in sensor readings and leading to control issues.

The rotor power electronic converters can cause a change in the current waveforms of the motor, which affects the accuracy of the rotor resistance variation (Abdelfattah and Ahmed, 2002). The three phase rectifier bridge in the rotor circuit of a slip ring induction motor causes harmonic currents in rotor circuit, these harmonic components are reflected to the stator circuit by electromagnetic transformation action and induce

* Corresponding Author:

Hilmi Fadhil Ameen

E-mail: hilmi.ameen@su.edu.krd

Article History:

Received: 19/02/2023

Accepted: 25 /04//2023

Published: 25 /10/2023

currents of corresponding frequencies in the stator winding (Outeiro and Saraiva, 2006). The stator current harmonics and torque pulsation have been analyzed for wound rotor induction motor speed control by resistance variation in rotor circuit side (Ameen, 2007). (Wang et al., 2008) implemented a rotor chopper controlled doubly fed induction machine by using the automated state model generator (ASMG) of a system in MATLAB/Simulink.

The simplest method used for controlling the speed of a slip ring induction motor is to convert a small amount of power into outer side impedance, as a result the motor current and total energy consumption are reduced (Ameen, 2011a). The power factor and rotor current distortion have been improved by third harmonic current injection in the rotor side of static rotor resistance variation, and the THD of rotor current has been reduced from 25% to 3% (Ameen, 2011b).

(Kumar et al., 2017) presented the speed control of wound rotor induction motor by static rotor resistance variation using MATLAB/Simulink for rotor chopper resistance and slip power recovery induction motor. (Bhardwaj et al., 2019) have investigated the performance of wound rotor induction motors with different configurations of the PWMVSI and buck-boost chopper. The proposed configurations have improved the power factor and efficiency and reduced of the THD of the power supply. (Bajjuri and Jain, 2018) investigated torque pulsation evaluation and reduction in a vector that controlled the slip ring induction motor double feed using different pulse width modulation approaches on both the stator and rotor side voltage source inverters.

The authors in (Bajjuri and Jain, 2018) demonstrated torque pulsation estimation and minimization in a vector that controlled the wound rotor induction motor double inverter feed using various pulse width modulation approaches on both the stator and rotor side voltage sources. (Adekitan and Abdulkareem, 2019) investigated the impact of the positive sequence voltage component variation on the motor losses, output power and sensitivity of three phase induction motor parameters. (El-Kharashi et al., 2019) examined the characteristics and efficiency of two unlike types of induction motors that are mechanically coupled and operated under

balanced and unbalanced voltages. (Donolo et al., 2020) showed a comparison of derating factors supplied by IEEE and NEMA standards to keep losses at the rated value. A complete mathematical model of SRRVIMDS is explained to investigate the effects of both three-phase bridge rectifier and chopper circuit converters and the interaction between the fundamental and the harmonics of stator and rotor currents on the harmonics of the electromagnetic torque under different unbalanced supply conditions presented by (Hilmi and Fadhil, 2021). Reference (Ameen and Aula, 2021) suggested the steady state mathematical modeling of SKIMDS based on ac circuit under different unbalance conditions. (Tabora et al., 2021) presented a comparison between energy efficiency and low power quality through a detailed of voltage unbalance with different motor classes.

In this paper, the harmonic analysis of SRRVIMDS is explained to investigate the effects of both three-phase bridge rectifier and chopper circuit converters and the interaction between the fundamental and the harmonics of stator and rotor currents on the harmonics of the electromagnetic torque under different unbalanced supply voltage conditions.

2. Harmonic Analysis of SRRVIMDS due to Rotor Power Electronic Converters

In most three-phase power semiconductor devices, harmonics are produced in orders of (x,y) on the direct current side and order of $(xy\pm 1)$ in the rotor winding, where x is an integer number and y is the number of pulses of a three-phase bridge rectifier. In a reliable drive system, the harmonic components cannot be ignored, otherwise, they lead to serious errors in the determination of the desired speeds, developed torque and the behavior of the drive system. The SRRVIMDS is different from most induction motor drives, in which the three-phase bridge rectifier and chopper circuit are connected to the rotor side instead of the stator side, as shown in Fig. 1, where R_{out} is the outside inserted resistance. The presence of a three-phase rectifier bridge in the rotor circuit causes harmonic currents in the rotor winding currents, and these harmonics are reflected in the stator winding currents by transformation action. As a result, machine losses are increased, and harmonic torques are developed. A per phase equivalent

circuit of SRRVIMDS referred to the stator side is shown in Fig. 2. Where R_{rh} is represented of the rotor harmonic resistance, $R_{eff}(\lambda)$ is effective ac

resistance in rotor side, R_s is stator resistance, X_r is the rotor reactance, and X_m is the magnetizing reactance per phase.

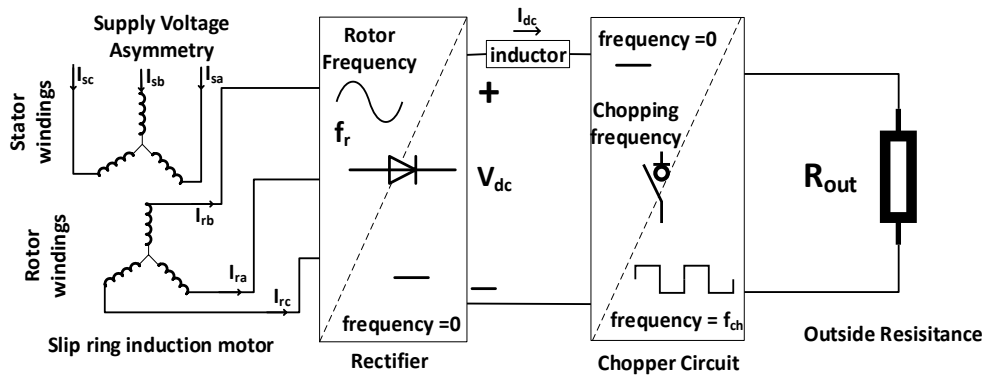


Fig. 1. The SRRVIMDS scheme

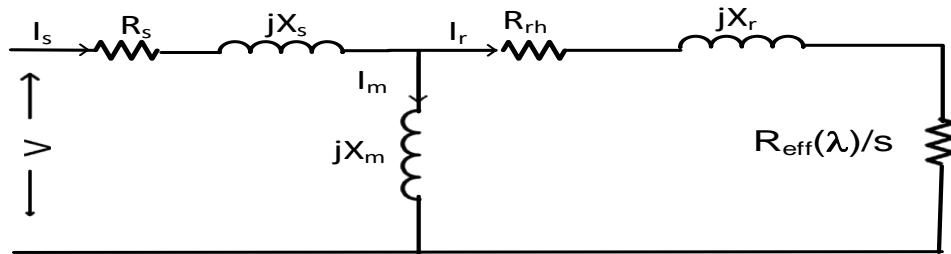


Fig. 2. The per Phase AC equivalent circuit model of SRRVIMDS

The Fourier series analysis of an alternating square pulse of (120°) degree duration shows that the rms value of the n^{th} harmonic current component is about (I_r/n) . These harmonic components produce additional copper losses, and

the magnitude of these currents depends on the speed of the motor. If the waveform of the rotor current is assumed to be a rectangular rotor current referred to the stator side as a sum of Fourier series components yields;

$$i_{ra}(\omega t) = 1.1I_{dc} \sin(s\omega t) - 0.023I_{dc} \sin(5s\omega t) + 0.024I_{dc} \sin(7s\omega t) - 0.022I_{dc} \sin(11s\omega t) + 0.024I_{dc} \sin(13s\omega t) - 0.02I_{dc} \sin(17s\omega t) + 0.018I_{dc} \sin(19s\omega t) + \dots \quad (1)$$

The magnitude of the n^{th} rotor current can be given by,

$$I_{rn} = \frac{\sqrt{6}}{n\pi} I_{dc} \quad (2)$$

In a three-phase bridge rectifier, there are six-pulses, and the harmonic frequencies at the dc side of the rotor which are equal to $6f_r$. While the rotor current frequency is (sf_s) , and s is the slip. The harmonic frequency of the dc side due to the diode rectifier will be;

$$f_{ach} = 6xsf_s \quad \text{where } x = 1, 2, 3 \dots \quad (3)$$

The rotor current harmonic components that are caused by 3-phase bridge rectifiers are given by (Papathanassiou and Papadopoulos, 2001):

$$f_{rh} = (1 \pm 6x)sf_s \quad \text{where } x = 1, 2, 3 \dots \quad (4)$$

From Eq. 4, where ($x=0$, is for the rotor fundamental components and $x=1$ is for harmonic orders of 5th, 7th). The presence of the three-phase bridge rectifier in the SRRVIMDS introduces harmonic currents in the rotor circuit. It is known that the $(6x+1)$ harmonics of the rotor current establish a positive sequence rotating magnetic field in the same direction as the fundamental mmf, while the $(6x-1)$ harmonics set up a negative sequence mmf. For motoring mode, the fundamental rotor mmf rotates in the same direction as the rotor and the relative angular speed between them is $(1\pm 6x)s_f$.

$$f_{sh} = (1 \pm 6xs)f_s \quad \text{where } x = 1, 2, 3 \dots \tag{5}$$

The interaction of rotating field waves produced by the stator and rotor fundamental and harmonic currents may be used to explain the electromagnetic harmonic torque. A steady nonzero average torque is created by traveling mmf waves that are stationary to one another. The relative speed of each mmf has a frequency of $(1 \pm 6xs)f_s$. When the absolute value is removed, the predicted electromagnetic torque harmonics are as follows:

$$f_{T,h} = \pm 6xsf_s \quad \text{where } x = 0, 1, 2, \dots \tag{6}$$

3. The SRRVIMDS Stator Current Harmonic Analysis

A per phase harmonic equivalent circuit referred to the rotor winding as the primary, which is injecting voltage at slip (s_n) to the stator winding

circuit, and the frequency of the stator is now divided by $((1\mp(n\pm 1) s)/(ns))$, resulting in an equivalent circuit of SRRVIMDS in Fig. 3.

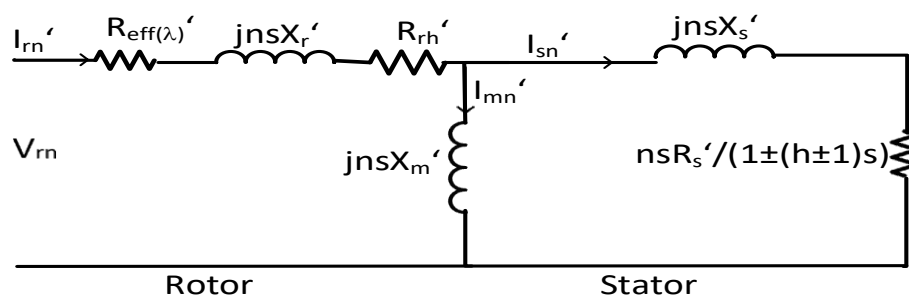


Fig. 3. The per phase harmonic equivalent circuit referred to stator side of SRRVIMDS.

From the harmonic equivalent circuit of Fig. 3, the harmonic stator current I_{sn} is induced by the n^{th} rotor current harmonic I_m and is given by;

$$= I'_{rn} \frac{jnsX'_m}{nsR'_s/(1\pm(h\pm 1)s) + jsn(X'_m + X'_s)} \tag{7} \quad I'_{sn}$$

Eq. 7 shows that the phase angle and peak value of the stator harmonic current can be founded for various speeds. Low harmonic orders, such as the 5th and 7th, will have a considerable value. Each harmonic component in the rotor winding will induce a flux of magnitude, the direction of which is calculated by the harmonic's order. The 5th

harmonic current rotates in the opposite direction of the rotor with a frequency of $5sn_s$, whereas the 7th harmonic rotates in the same direction at a frequency of $7sn_s$. The 5th order rotor harmonic current generates a magnetic field in the air gap that spins at $(-5sn_s)$ relative to the rotor $ns(1-s)$. As a consequence, the 5th harmonic rotating field speed with regard to the stator is $[n_s(1-s) + (-5sn_s)] = n_s(1-6s)$. As a result, the rotor-induced stator current has a frequency of $(1-6s) f_s$.

The harmonic forced into the rotor by the rectification process produces electromagnetic pulsating torque, which can be derived by considering the case of the 5th and 7th harmonics of rotor current injected into the stator as in Eq. 7.

Where $= \frac{n_1 \pi^2 I_{r1} (R_m(s) + R_{out} - f_{ch} R_{out} T_{on})}{18 V}$, f_{ch} is the chopper frequency, T_{on} is the ON period of chopper cycle $R_m(s) = \left(2R'_s + \frac{3(X'_m + X'_r)}{\pi} s + 2R_r \right)$ and n_1 is the stator to rotor turn ratio.

$$T_{s5} = 3 \left(\frac{I_{r1}}{5} \right)^2 \frac{X'_m{}^2 R'_s}{(1-6s)\omega_s \left[\left(\frac{R'_s}{(1-6s)} \right)^2 + (X'_m + X'_s)^2 \right]}$$

$$= 3 \left(\frac{I_{r1}}{5} \right)^2 \frac{X'_m{}^2 R'_s}{\left(1 - \frac{\pi^2 I_{r1} [R_m(s) + R_d + R_{out}(1-\lambda)] n_1}{3V} \right) \omega_s \left[\left(\frac{R'_s}{1 - \frac{\pi^2 I_{r1} [R_m(s) + R_d + R_{out}(1-\lambda)] n_1}{3V}} \right)^2 + (X'_m + X'_s)^2 \right]} \quad (8)$$

$$T_{s7} T_{s7} = 3 \left(\frac{I_{r1}}{7} \right)^2 \frac{X'_m{}^2 R'_s}{(1+6s)\omega_s \left[\left(\frac{R'_s}{(1+6s)} \right)^2 + (X'_m + X'_s)^2 \right]}$$

$$= 3 \left(\frac{I_{r1}}{7} \right)^2 \frac{X'_m{}^2 R'_s}{\left(1 - \frac{\pi^2 I_{r1} [R_m(s) + R_d + R_{out}(1-\lambda)] n_1}{3V} \right) \omega_s \left[\left(\frac{R'_s}{1 - \frac{\pi^2 I_{r1} [R_m(s) + R_d + R_{out}(1-\lambda)] n_1}{3V}} \right)^2 + (X'_m + X'_s)^2 \right]} \quad (9)$$

It's clear from eqs. 8 and 9 that the harmonic torques for 5th and 7th are functions of the slip, or with duty cycle (λ) of the rotor chopper circuit and they are small compared to the torque caused by the rotor current. The rotor fundamental current I_{rf} based on the approximate equivalent circuit at supply frequency for SRRVIMDS can be written as:

$$I'_{r1} \approx \frac{V}{n_1 \sqrt{\left(R'_s + \frac{R_d + R_{eff}(\lambda)}{s} \right)^2 + (X'_1 + X'_2)^2}} \quad (10)$$

The fundamental torque based on the approximate equivalent circuit approximately can be written as follows:

$$T_f = \frac{3 \left(\frac{V}{n_1} \right)^2 \left(R'_s + \frac{R_d + R_{eff}(\lambda)}{s} \right)}{\omega_s \left[\left(R'_s + \frac{R_d + R_{eff}(\lambda)}{s} \right)^2 + (X'_1 + X'_2)^2 \right]} \quad (11)$$

The ratio of the 5th and 7th harmonic torque to fundamental torque are;

$$\frac{T_{s5}}{T_f} \approx 0.04 * \frac{X'_m{}^2 R'_s}{(1-6s) \left[\left(\frac{R'_s}{(1-6s)} \right)^2 + (X'_m + X'_s)^2 \right]} * \frac{s}{sR'_s + R_d + R_{eff}(\lambda)} \quad (12)$$

The ratio of the 7th harmonic torque to fundamental torque is;

$$\frac{T_{s7}}{T_f} \approx 0.02 * \frac{X'_m{}^2 R'_s}{(1+6s) \left[\left(\frac{R'_s}{(1+6s)} \right)^2 + (X'_m + X'_s)^2 \right]} * \frac{s}{sR'_s + R_d + R_{eff}(\lambda)} \quad (13)$$

The highest ratio of values of 5th harmonic electromagnetic torque to full load torque occurs near $s=0.16$; this ratio is positive at $s < 0.16$ and negative beyond it. The value of $R'_s \leq R_d + R_{eff}(\lambda)$ and the other term are less than one; therefore, the ratio is never larger than 4%. Similarly, the maximum ratio for 7th harmonic torque to fundamental occur when $s=0.16$, the ratio is positive as $s < 0.16$ and negative when $s > 0.16$. Also, the value of $R'_s \leq R_d + R_{eff}(\lambda)$ and

the other terms are less than one, therefore, the ratio is never greater than 2%. The torque produced by other harmonics, like 11th, 13th, 17th, 19th, 23th, 25th, can be calculated by the same method, but the values are very low.

4. Results and Discussion

A 400V, 1.8kW, 4-pole, wound rotor induction motor has been used under the unbalanced supply voltage for different values of the voltage unbalance factor. The presence of a

three-phase bridge rectifier and a chopper circuit in the rotor circuit of WRIM causes harmonic currents in the rotor, and these harmonics have been reflected to the stator by transformation action. As a result, the machine losses are increased, and harmonic pulsation is developed.

Fig. 4 shows the Simulink/ Matlab model implementation for SRRVIMDS. Figs. 5 ,6 and 7 show the rotor injected stator current, rotor current, and electromagnetic torque harmonic

spectrum of SRRVIMDS for VUF of 0%, 5%, and 10% when $\lambda=0.75$ for the proposed mathematical model and fast Fourier transform (FFT) MATLAB simulation. It can be noted that the frequencies for the analytical solution and FFT Matlab and with their corresponding amplitude values, have a very small deviation and are in the acceptable range.

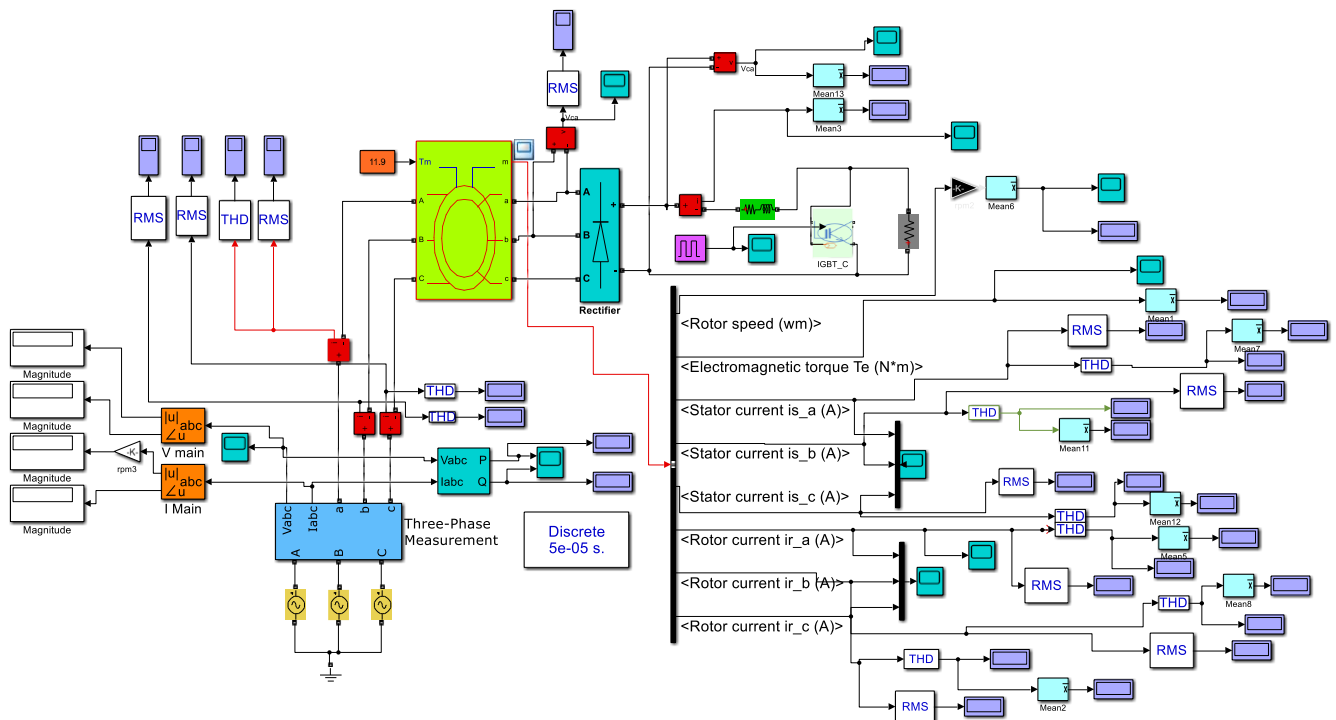


Fig. 4 The Simulink model of SRRVIMDS under asymmetry supply voltages.

Figs. (4, 5 and 6) a and b show the rotor injected stator current harmonic for mathematical evaluation and FFT MATLAB simulation results are shown in table 1 for (VUF= 0%) (s=0.2), (VUF = 5%)(s=0.22) and (VUF = 10%) (s=0.246) when the duty cycle of the chopper circuit is adjusted on 0.75.

Figs. (4, 5 and 6) c and d show the rotor current harmonic components for mathematical calculation and FFT MATLAB simulation results are shown in table 2 for (VUF= 0%) (s=0.2), (VUF = 5%)(s=0.22) and (VUF = 10%) (s=0.246) when the duty cycle of the chopper circuit is adjusted on 0.75.

Figs. (4, 5 and 6) e and f show the electromagnetic torque spectrum components for mathematical calculation and FFT MATLAB simulation results are shown in table 3 for (VUF= 0%) (s=0.2), (VUF = 5%)(s=0.22) and (VUF = 10%) (s=0.246) when the duty cycle of the chopper circuit is adjusted on 0.75.

Table 1: Stator current amplitude rotor injected variation for different harmonic orders

x	VUF = 0%, (s=0.2)			VUF = 5%, (s=0.22)			VUF =10%, (s=0.246)		
	/f/ (Hz)	Theor. (A)	FFT (A)	/f/ (Hz)	Theor. (A)	FFT (A)	/f/ (Hz)	Theor. (A)	FFT (A)
0	50	6.06	5.8	50	6.1	5.6	50	6.3	5.8
1	10	0.6	0.56	16	0.65	0.61	23.8	0.7	0.74
	110	0.42	0.4	116	0.45	0.44	123.8	0.49	0.51
2	70	0.28	0.29	82	0.32	0.36	97.6	0.35	0.43
	170	0.22	0.21	182	0.23	0.23	197.6	0.27	0.29
3	130	0.18	0.17	148	0.21	0.21	171.4	0.24	0.25
	230	0.15	0.14	248	0.17	0.16	271.4	0.2	0.2
4	190	0.12	0.11	214	0.14	0.13	245.2	0.165	0.162
	290	0.1	0.1	314	0.13	0.12	345.2	0.15	0.14
5	250	0.11	0.09	280	0.12	0.11	319	0.14	0.13
	350	0.08	0.07	380	0.11	0.1	419	0.13	0.12

Table 2: Rotor current amplitude variation for different harmonic orders

x	VUF = 0%, (s=0.2)			VUF = 5%, (s=0.22)			VUF =10%, (s=0.246)		
	/f/ (Hz)	Theor. (A)	FFT (A)	/f/ (Hz)	Theor. (A)	FFT (A)	/f/ (Hz)	Theor. (A)	FFT (A)
0	10	4.46	4.5	11	4.7	4.71	12.3	5.02	4.9
1	50	0.85	0.88	55	0.92	0.91	61.5	0.95	0.98
	70	0.62	0.68	77	0.64	0.75	86.1	0.74	0.86
2	110	0.39	0.43	121	0.4	0.47	135	0.43	0.53
	130	0.31	0.32	143	0.34	0.33	160	0.36	0.38
3	170	0.25	0.27	187	0.26	0.3	209	0.28	0.29
	190	0.22	0.22	209	0.23	0.23	234	0.25	0.26
4	230	0.15	0.14	253	0.19	0.16	283	0.21	0.2
	250	0.14	0.13	275	0.12	0.11	307	0.19	0.19
5	290	0.11	0.12	319	0.15	0.14	356	0.16	0.15
	310	0.09	0.07	341	0.14	0.12	381	0.12	0.12

Table 3: The torque developed amplitude variation for different harmonics

x	VUF = 0%, (s=0.2)			VUF = 5%, (s=0.22)			VUF =10%, (s=0.246)		
	f (Hz)	Theor. (N.m)	FFT (N.m)	f (Hz)	Theor. (N.m)	FFT (N.m)	f (Hz)	Theor. (N.m)	FFT (N.m)
0	0	12	12.01	0	11.99	11.95	0	11.98	11.93
1	60	0.95	1.04	66	0.96	1.06	73.8	1.02	1.07
2	120	0.22	0.192	132	0.235	0.24	147.6	0.251	0.23
3	180	0.1	0.102	198	0.106	0.096	221.4	0.109	0.101
4	240	0.05	0.048	264	0.058	0.04	295.2	0.064	0.051
5	300	0.03	0.025	330	0.037	0.028	369	0.04	0.031

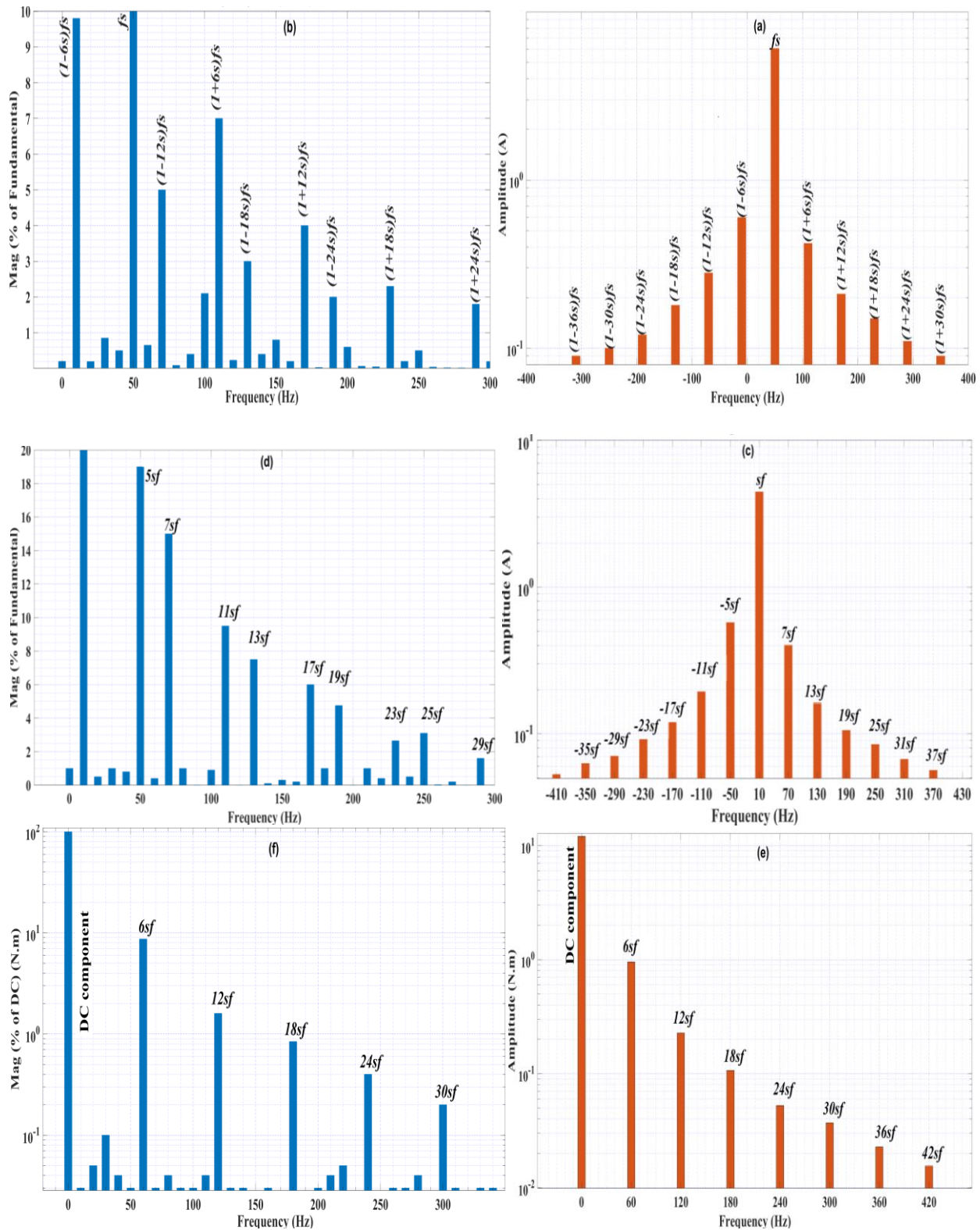


Fig. 5: Amplitude value for VUF=0%, $\lambda=0.75$ and speed of 1200rpm for, (a) Stator current (mathematical model), (b) Stator currents (FFT), (c) Rotor currents (mathematical model), (d) Rotor current (FFT), (e) Torque (mathematical model), and (f) Torque (FFT)

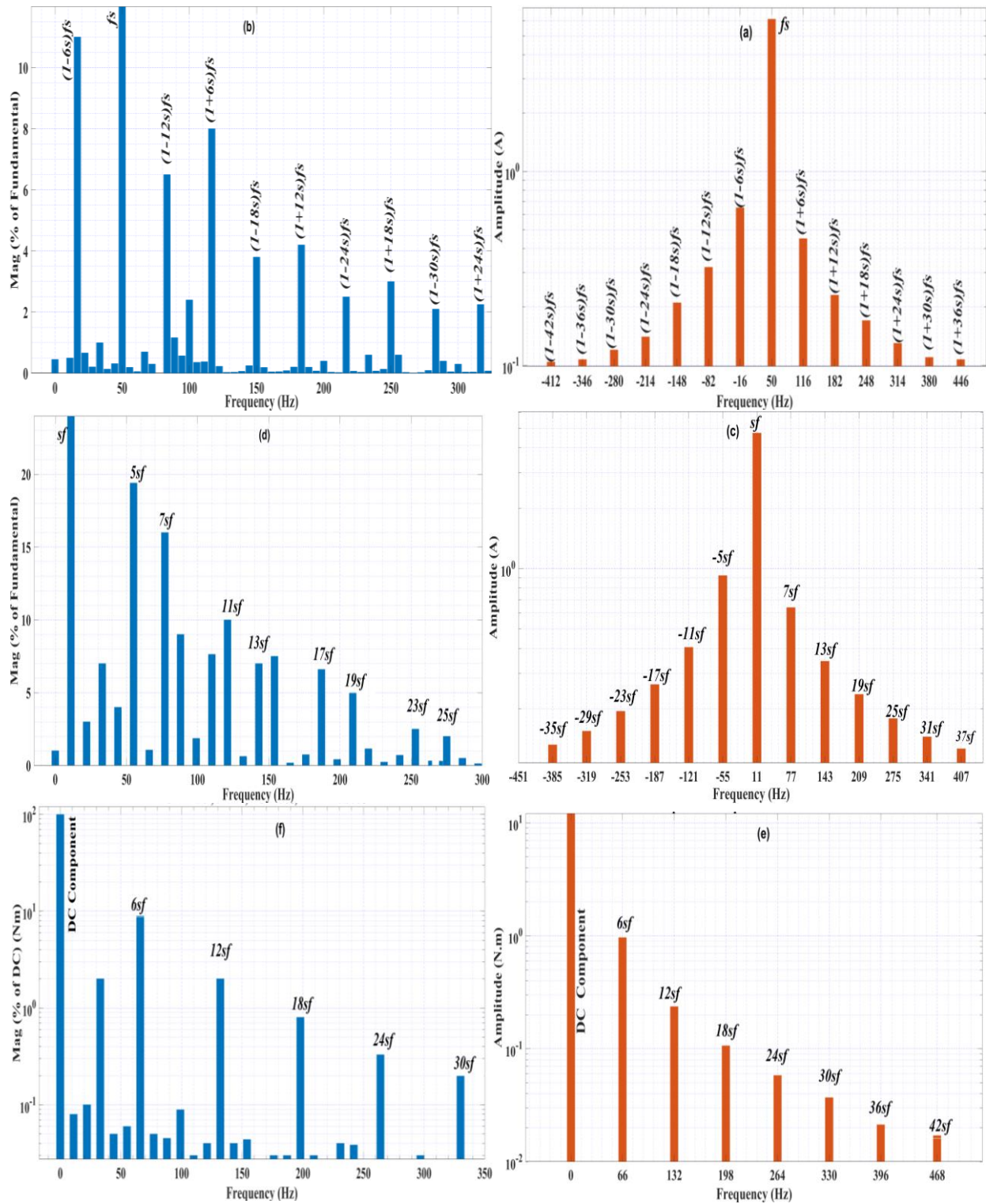


Fig. 6: Amplitude value for VUF=5%, $\lambda=0.75$ and speed of 1170 rpm for, (a) Stator current (mathematical model), (b) Stator currents (FFT), (c) Rotor currents (mathematical model), (d) Rotor current (FFT), (e) Torque (mathematical model), and (f) Torque (FFT)

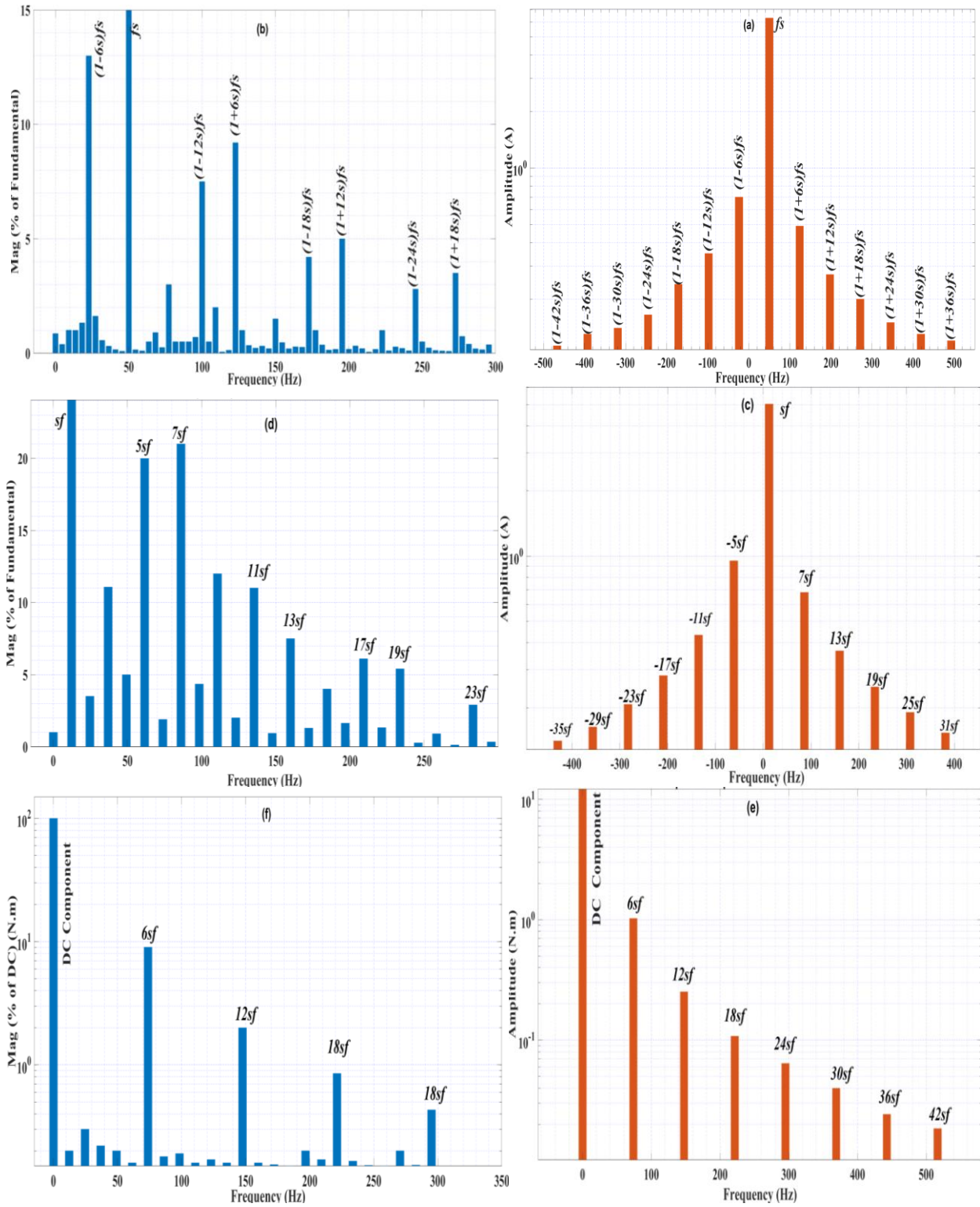


Fig. 7: Amplitude value for VUF=% 10, $\lambda=0.75$ and speed of 1131 rpm for, (a) Stator current (mathematical model), (b) Stator currents (FFT), (c) Rotor currents (mathematical model), (d) Rotor current (FFT), (e) Torque (mathematical model), and (f) Torque (FFT)

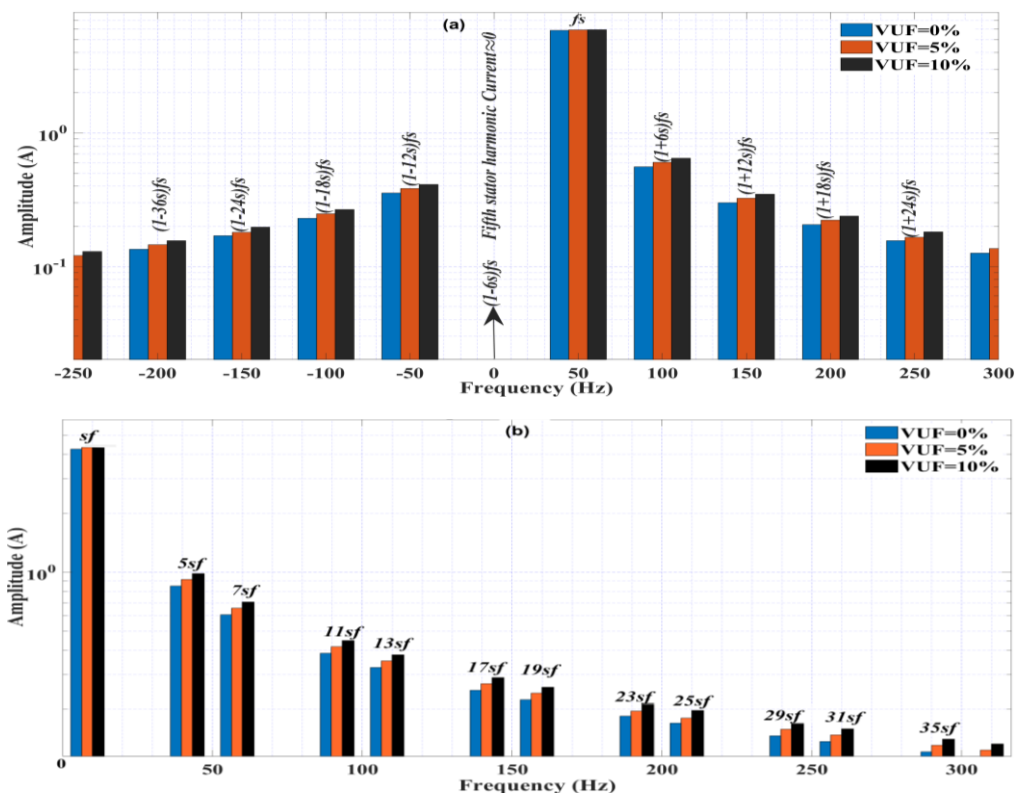
Fig. 8 shows the harmonic spectrum for rotor injected stator current, rotor currents, and torques from the mathematical calculation for (0, 5, 10)% of VUF and slip of 0.1666 (1250rpm), respectively. The rotor speed can be controlled by changing the duty cycle of the chopper circuit. Based on Eq. 7 ($n=5$), a special case occurs relevant to a certain combination of ($s=1/6$). The rotating mmf produced by the 5th harmonic of the rotor current at standstill at $s=1/6$ and therefore does not induce a corresponding harmonic in the stator windings. In this case, it can be seen that the 5th harmonic induced on the stator side due to rotor harmonic mmf is zero.

The spectrum harmonic analysis and Fourier transform of stator current in Fig. 8 yield a insignificant harmonic components at this slip. When the speed is a multiple of 1/6, the three-phase diode bridge rectifier in the rotor side causes a unique occurrence related to the synchronization of the motor space harmonics with the diode rectifier commutation. This synchronization has an impact on the currents in

the rotor and stator, as well as the pulsation of the resulting torque.

Fig. 8a shows the injected stator current rotor, rotor current, and electromagnetic torque harmonics spectrum for SRRCCIM for 0%, 5%, and 10% of VUF of supply voltage and rotor speed of 1250 rpm as they are obtained from FFT MATLAB simulation.

It is noted that the amplitude of the injected stator current rotor is increased with increasing VUF, and we can also observe that the 5th harmonic order of the rotor current has not affected the stator current at $s = 1/6$ exactly, and it is equal to zero. Fig. 8b shows the harmonics that are produced by the chopper circuit and rotor rectifier for the same slip in rotor winding, and also shows how these currents are affected by the asymmetry of supply voltages. Similarly, the electromagnetic torque that is developed by the system is affected by the supply voltage asymmetry, and the amount of torque pulsation is increased with increasing VUF, as shown in Fig. 8c.



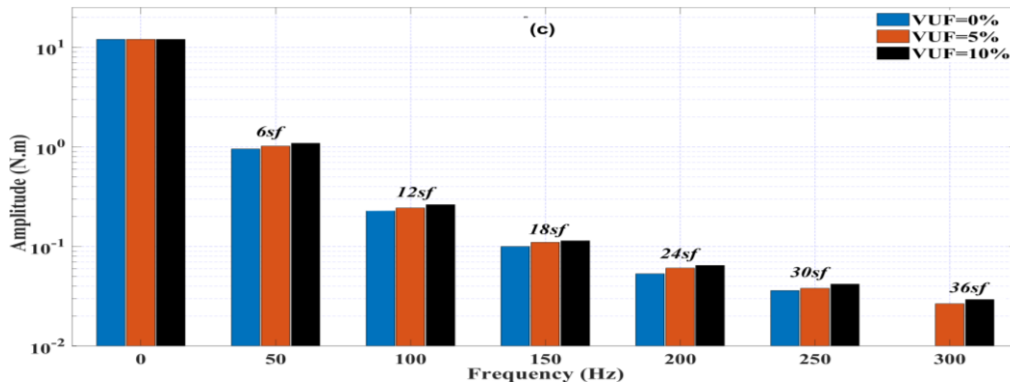


Fig. 8: Amplitude value of (a) Stator current, (b) Rotor current, (c) Torque at speed of 1250rpm.

Figs. 9a and 9b show the rotor injected stator rms current for harmonics order 5th, 7th, 11th, and 13th for analytical calculation against slip and speed for VUF of 0%, 5%, and 10%, respectively. It can be seen that from standstill to about no-load slip, the 7th and 13th harmonic orders currents are approximately constant, while the 5th harmonic order rotor injected stator current is zero at $s=1/6$, and similarly, the 11th harmonic order rotor injected stator current is equal to zero at $s=1/12$ for VUF = 0%, 5 %, and 10%, respectively.

Figs. 10a, 10b, 10c, and 10d show the electromagnetic torque that is developed by the 5th, 7th, 11th and 13th harmonic orders due to rotor injected stator current for VUF = 0% and 10% and duty cycles of 0.5 and 1, respectively. Also, the torque that is developed in the 5th order at $s=1/6$ in

Fig. 10a and the 11th order at $s=1/12$ in Fig. 10c is zero.

The torque that is developed by rotor injected stator currents of 7th and 13th harmonic orders is increased by increasing the λ , while it decreases with increasing the VUF%. In contrast, for harmonic torques of 5th and 11th increasing orders, the λ tends to decrease T_{e5} and T_{e11} , while the effect of VUF is the same as T_{e7} and T_{e13} . Fig. 10e shows the resultant torque that is developed by harmonics of the 5th, 7th, 11th, and 13th orders versus the speed for 0.5 and unity duty cycle. It can be seen that the amounts of T_{e7} , T_{e11} , and T_{e13} are very small in comparison with T_{e5} .

Fig. 10f shows the fundamental torques T_{e1} and T_{e5} , T_{e7} , T_{e11} , and T_{e13} versus the speed for VUF variation between 0% and 10% for $\lambda = 0.5$. It can be noted that the effect of rotor injected stator current is clear, but it is not significantly high to affect the performance.

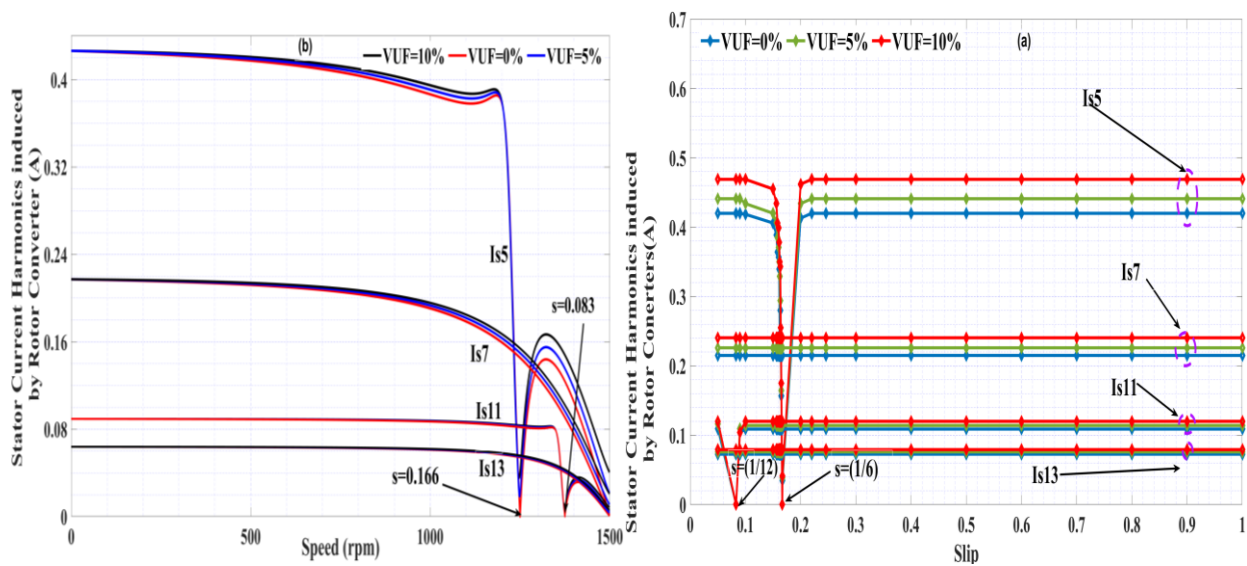


Fig. 9: (a) Rotor injected stator current harmonics ($\lambda=0.75$)(mathematical), (b) Rotor injected stator current harmonics ($\lambda=0.75$)(simulation)

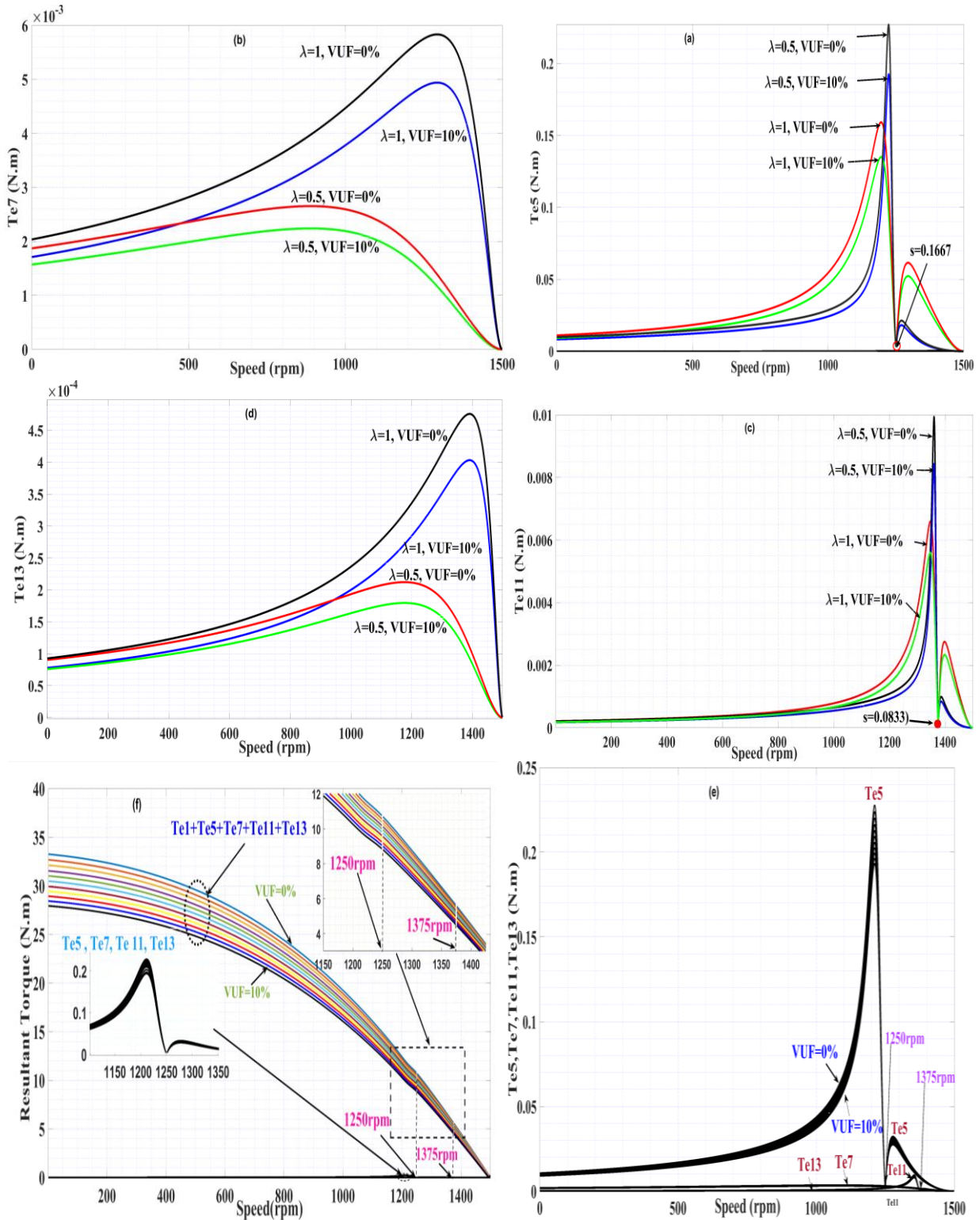


Fig.10: (a) T_{e5} (VUF=0 and 10% with $\lambda=0.5$ and 1), (b) T_{e7} (VUF=0 and 10% with $\lambda=0.5$ and 1), (c) T_{e11} (VUF=0 and 10% with $\lambda=0.5$ and 1), (d) T_{e13} (VUF=0 and 10% with $\lambda=0.5$ and 1), (e) $T_{e5}+T_{e7}+T_{e11}+T_{e13}$ (VUF=0 and 10%)($\lambda=0.75$), (f) T_e (Resultant)($\lambda=0.75$).

Figs. 11a and 11b show the electromagnetic torque developed response at $s=1/6$ for voltage unbalance factor of 0% and 10%, respectively. It can be seen that the peak to peak torque pulsation for 0% of VUF is 3 N.m and equal to 5.5 N.m for 10% of VUF.

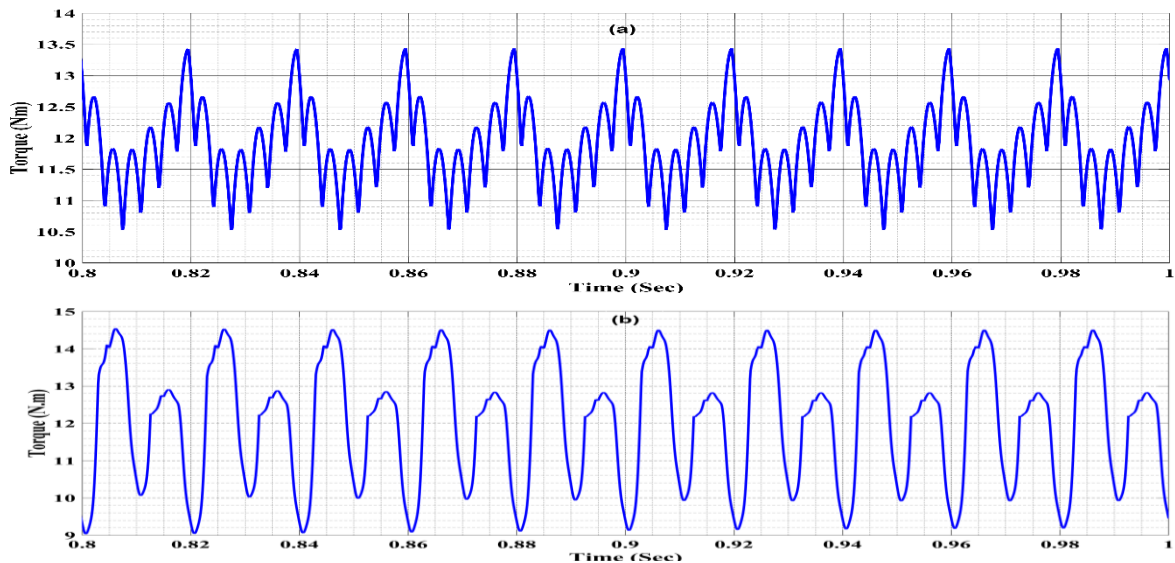


Fig.11: The electromagnetic torque response at $s=1/6$, (a) (VUF=0%) and (b) (VUF=10%).

Figs. 12a and 12b show the ripple in rotor speed for VUF of 0% and 10%, respectively. It can be shown that the speed ripple is 3 rpm, while the VUF is 10% the speed ripple is 7 rpm. Figs. 13a and 13b show the ripple in electromagnetic torque for VUF of 0% which is 2.5N.m ($s=0.2$) and when VUF is 10%, it is 4.2N.m ($s=0.246$) at $\lambda=0.75$.

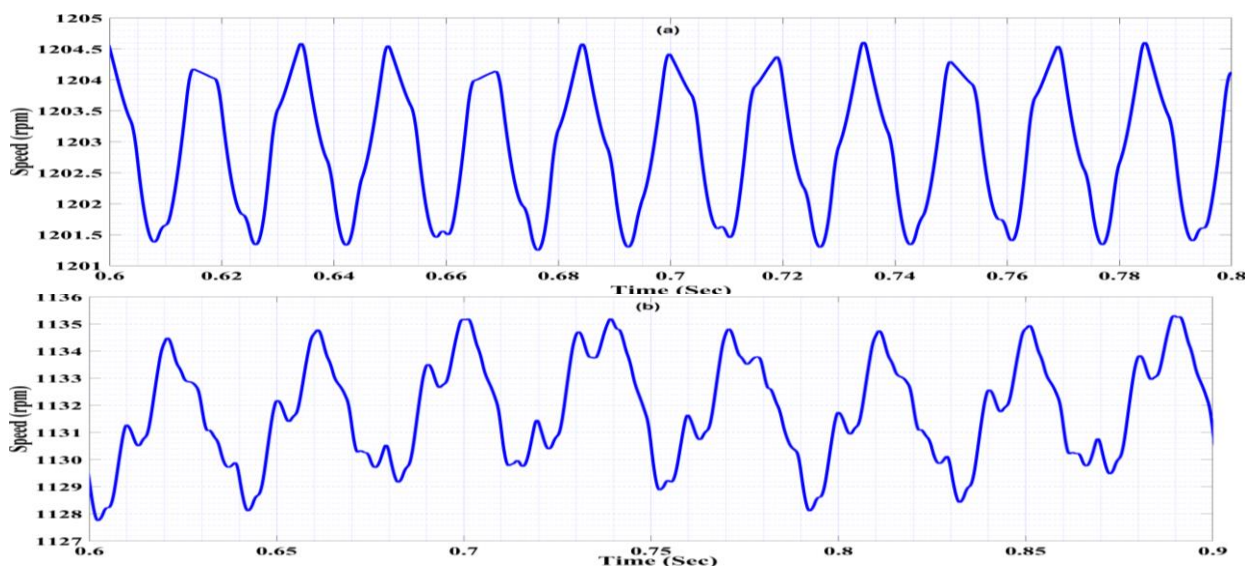


Fig.12: The Rotor speed response at $\lambda=0.75$, (a) (VUF=0%) and (b) (VUF=10%).

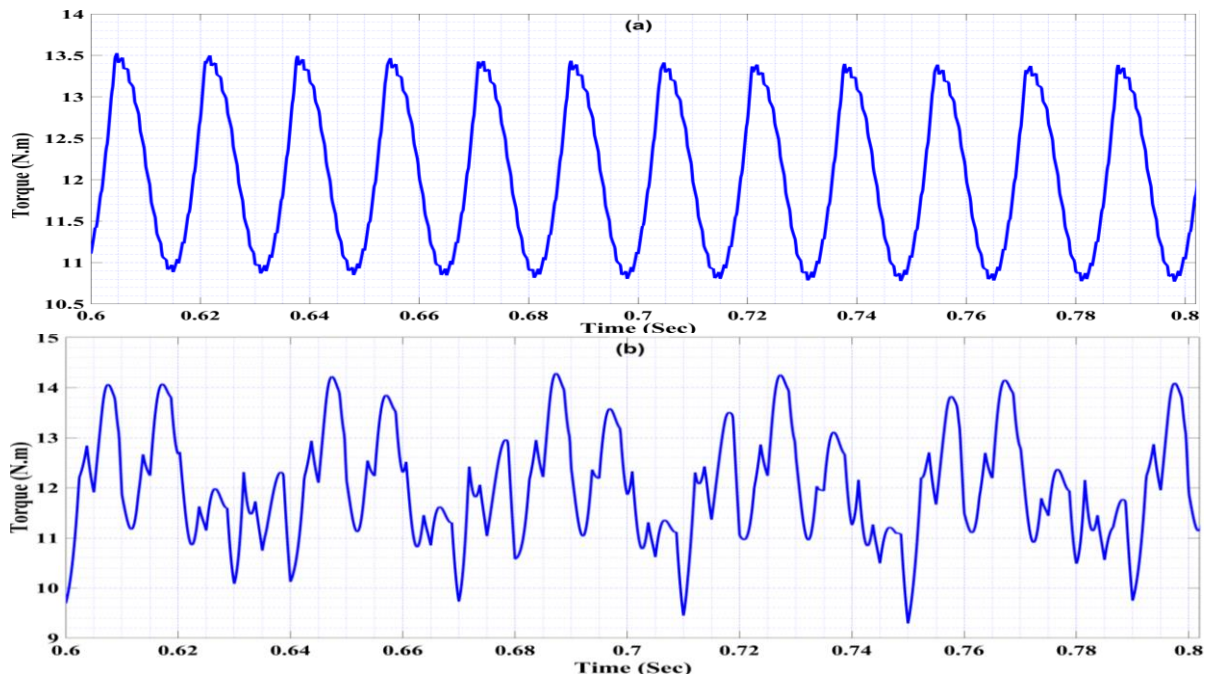


Fig.13: The electromagnetic torque response at $\lambda=0.75$, (a) (VUF=0%) and (b) (VUF=10%).

5. CONCLUSION

This paper investigated and evaluated the performance of SRRVIMDS under asymmetrical supply voltages. The proposed mathematical model and SIMULINK/ MATLAB are used for evaluating and verifying the conditions. Whereas SRRVIMDS operates under unbalanced supply voltage conditions, the characteristics of the drive will be changed. Distortion currents are caused by rotor currents in the stator windings at frequencies that are not an integral multiple of the supply frequency, especially at $s=1/6$ and the equivalent circuit for the corresponding rotor current harmonics has been used to determine these distortion currents independently. By adding these distortion currents, the stator current waveform will be produced. The most pronounced impacts of an unbalanced supply voltage are the increased heating due to additional losses. These losses are dissipated in the stator and rotor windings, and consequently, the developed torque and efficiency of SRRVIMDS are decreased.

6. References

- ABDELFATTAH, M. & AHMED, M. An artificial neural network-based chopper-controlled slip-ring induction motor. 11th IEEE Mediterranean Electrotechnical Conference (IEEE Cat. No. 02CH37379), 2002. IEEE, 142-146.
- ADEKITAN, A. I. & ABDULKAREEM, A. 2019. The significance of the mode of voltage imbalance on the operation and energy losses of a 3-phase induction motor. *Engineering and Applied Science Research*, 46, 200-209.
- AMEEN, H. F. 2007. Stator Current Harmonic Analysis and Torque Pulsation of Wound Rotor Induction Motor Speed Control by Chopper Resistance in Rotor Circuit. *Zanco Journal of pure and Applied Science*, 19, 123-134.
- AMEEN, H. F. 2011a. Computer simulation and mathematical modelling of static rotor resistance chopper control of WRIM by reference frame theory. *Procedia Computer Science*, 3, 1009-1017.
- AMEEN, H. F. 2011b. Minimizing Rotor Current Distortion and Power Factor Improvement of WRIM Chopper Resistance Control Using Third Harmonic Current Injection. *Zanco Journal of pure and Applied Science* 23, 23-37.
- AMEEN, H. F. & AULA, F. T. 2021. Performance Analysis of the Slip Power Recovery Induction Motor Drive System Under Unbalance Supply Voltages. *Advances in Electrical and Electronic Engineering*, 19, 192-202.
- BAJJURI, N. K. & JAIN, A. K. 2018. Torque Ripple Reduction in Double-Inverter Fed Wound Rotor Induction Machine Drives Using PWM Techniques. *IEEE Transactions on Industrial Electronics*, 66, 4250-4261.
- BHARDWAJ, S. R., RAHI, O. & SHARMA, V. 2019. Comparative Analysis of Induction Motor Drive with Chopper Controlled SPRS Employing Various Inverter Configurations. *IETE Journal of Research*, 65, 329-341.
- DONOLO, P. D., PEZZANI, C. M., BOSSIO, G. R., DE ANGELO, C. H. & DONOLO, M. A. 2020. Derating of induction motors due to power quality issues considering the motor efficiency class. *IEEE Transactions on Industry Applications*, 56, 961-969.

- EL-KHARASHI, E., MASSOUD, J. G. & AL-AHMAR, M. 2019. The impact of the unbalance in both the voltage and the frequency on the performance of single and cascaded induction motors. *Energy*, 181, 561-575.
- HILMI, A. & FADHIL, A. 2021. Performance Analysis and Modeling of SRRCCIM under the Impact of Unbalance Supply Voltage. *Journal of Electrical and Electronics Engineering*, 14, 5-10.
- KUMAR, R., DOGRA, R. & AGGARWAL, P. 2017. Rotor side speed control methods using MATLAB/Simulink for wound induction motor. *International Journal of Mechanical and Mechatronics Engineering*, 11, 1385-1393.
- OUTEIRO, M. & SARAIVA, E. 2006. Harmonics on the Electromagnetic Torque of a Slip Energy Recovery System with Two Thyristor Bridges and no DC Coil. University of Coimbra-Portugal, Internet Issued.
- PAPATHANASSIOU, S. & PAPADOPOULOS, M. 2001. On the harmonics of the slip energy recovery drive. *IEEE Power Engineering Review*, 21, 55-57.
- TABORA, J. M., TOSTES, M. E. D. L., BEZERRA, U. H., DE MATOS, E. O., PEREIRA FILHO, C. L., SOARES, T. M. & RODRIGUES, C. E. M. 2021. Assessing Energy Efficiency and Power Quality Impacts due to High-Efficiency Motors Operating under Nonideal Energy Supply. *IEEE Access*.
- WANG, L., CHINIFOROOSH, S. & JATSKEVICH, J. Simulation and analysis of starting transients in rotor-chopper-controlled doubly-fed induction motors. 2008 IEEE Canada Electric Power Conference, 2008. IEEE, 1-6.